

Effect of rock strength on failure mode and mechanical behavior of composite samples

Jie Liu · Enyuan Wang · Dazhao Song · Siheng Wang · Yue Niu

Received: 22 October 2013 / Accepted: 27 July 2014 / Published online: 19 August 2014
© Saudi Society for Geosciences 2014

Abstract Many dynamic events in coal mine are caused by the instability of coal–rock body. In order to study the influence of rock strength on this type of instability, uniaxial compression experiments of rock–coal–rock composite samples with different rock strengths are carried out, and the effect and mechanism of rock strength on the mechanical behavior and fracture mode of the composite samples are analyzed. The results show that major failure modes of the composite samples are conjugate X-shaped shearing fracture and splitting fracture. The angle between the shear fracture surface and the end face increases with rock strength. The splitting fracture in the coal body expands to the rock when the rock strength is low. The strength properties of the composite samples mainly depend on the coal strength instead of the rock strength. With the rock strength increasing, the peak strain of the composite samples decrease, and the differences from the coal strain and strain rate to rock strain and strain rate become greater. These failure modes and characteristics of deformation are shown to be determined by the difference between the elastic modulus of rock and coal constituting the composite samples.

Keywords Composite coal–rock sample · Rock strength · Stress–strain curve · Deformation law

E. Wang (✉) · D. Song · S. Wang · Y. Niu
Key Laboratory of Gas and Fire Control for Coal Mines, China
University of Mining and Technology, Xuzhou, Jiangsu, China
221116
e-mail: sihescience@163.com

E. Wang · D. Song · S. Wang · Y. Niu
Faculty of Safety Engineering, China University of Mining and
Technology, Xuzhou, Jiangsu, China 221116

J. Liu
Department of Safety Engineering, Qingdao Technological
University, Qingdao, Shandong, China 266520

Introduction

Coal–rock dynamic disaster is the sudden destruction or instability of coal–rock masses under load, including coal and gas outburst, rock burst, etc. (Lama and Bodziony 1998; Vesela 1996). During the process of mining, the destruction of coal–rock mass is influenced not only by their fracture surface, but also by the characteristics of the roof and floor rock (Qin et al. 2006; Paul et al. 2012; Bai et al. 2013; Zhang et al. 2014). In the late period of many collieries, many protective coal pillars and stopping coal pillars (Shabanimashcool and Li 2012; Singh et al. 2011; Liu et al. 2013) are left in the mining space, and the composite structure consisted of these coal pillars and overlying strata may determine the safety of the mining space. With the increase of mining depth, the roof and floor rock have larger effect on the stress in the coal bed (Hosseini et al. 2013; He et al. 2005) and it is necessary to study the deformation and fracture mechanism of the system composed of roof–floor rocks and coal.

The failure of rock samples in stress–strain testing is similar to the dynamic disasters in the field (Cook 1965; Bieniawski et al. 1969; Wawersik and Fairhurst 1970); however, the stiffness of the testing machine is much greater than that of the surrounding rocks in the colliery. In order to better simulate the actual instability of coal rock, many scholars combined two kinds of rocks with different properties to simulate the phenomenon of dynamic instability (Chen et al. 1997; Lin et al. 1999; Seidel and Haberfield 2005; Xie et al. 2005), and found that the stiffness of the rock part in series combination is closely related to micro-fracture migration, deformation localization, and post-peak fracture characteristics. To better simulate the complicated geological

and working condition of colliery, the fracture failure mode and strength were also investigated for coal–rock composite samples under different stress conditions (Zuo et al. 2011a), and with different geometrical sizes (Deng, et al. 2012), inclined angles (Guo, et al. 2011), modes of combination (Zhang, et al. 2012), and loading rates and paths (Zuo et al. 2011b; Huang and Liu 2013). These studies contribute to our knowledge about the mechanical behavior and fracture failure mode of composite samples.

Rock burst propensity is an important index to evaluate the probability of dynamic disaster, and the difference between this index of composite samples and coal or rock was studied by Li et al. (2005). The effect of height ratio (Liu et al. 2004), and strength and thickness (Dou et al. 2006; Lu et al. 2009, 2010) of coal and rock on this index were also investigated, and the rock burst propensity of composite sample was found to increase with the proportion of rock (in height and strength). These studies help to illustrate the relationship between the properties of coal–rock body and the energy released in fracture failure of composite samples.

Occasionally, different roof rock on top of the same coal seam in different mining areas may lead to varied dynamic behaviors of the coal seam. In the process of dynamic evolution, knowledge about the deformation of coal–rock mass is equally important as the development of fracture. In this paper, rocks with different strengths are selected to form composite samples with the same coal body, and the stress–strain curves, fracture failure mode, and deformation laws of these composite samples under uniaxial compression are tested and the intrinsic mechanisms of these mechanical behaviors are discussed.

Testing program

Sample preparation

The geologic model of the composite samples tested in this study is a coal wall in the Sijiazhuang coal mine located in Shanxi Province, China. The histogram of the target coal seam in Fig. 1 indicates that the rock strata with great influence on the deformation and stress of the coal seam are distributed approximately in the proportions of 3:4:3 (with the coal seam in the middle) in thickness. From the experimental perspective, if the rock part were too large, the fracture failure of the coal part would not be easily observed; if the coal part were too large, the influence of rock on the fracture failure of the coal part would be too small. Moreover, according to the ISRM standard (Fairhurst and Hudson 1999), “test specimens shall be right circular cylinders having a height -to-diameter

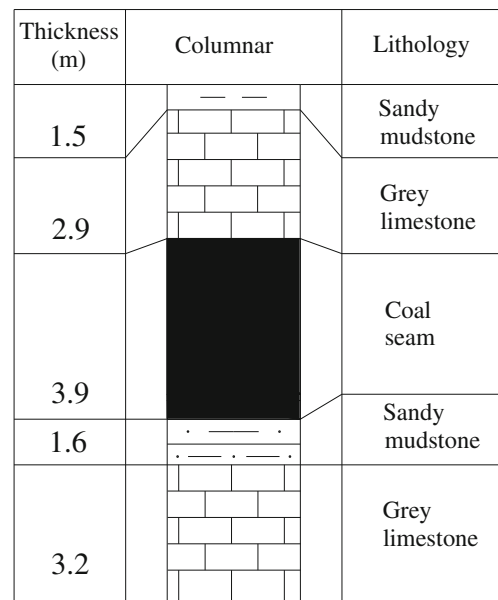


Fig. 1 Coal seam histogram

ratio of between 2.0 and 3.0 and a diameter preferably of not less than approximately 50 mm.” Finally, the sizes of the composite samples shown in Fig. 2 are selected.

Rock blocks with different strengths for testing are taken from the Sijiazhuang coal mine (SR) located in Shanxi Province, China; Xinlu coal mine (XR) located in Heilongjiang Province, China; Liangbei coal mine (LR) located in

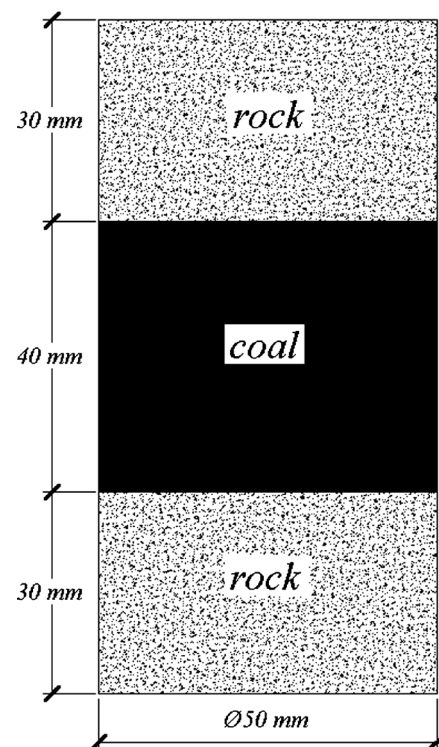


Fig. 2 Sketch map of composite sample

Henan Province, China; Jinhuangzhuang coal mine (JR) located in Anhui Province, China; and Da'anshan coal mine (DR) located in Beijing, and the coal blocks are from the Sijiazhuang coal mine (SC) located in Shanxi Province, China, all in sizes about $50\text{ cm}^3 \times 50\text{ cm}^3 \times 50\text{ cm}^3$. According to the International Society for Rock Mechanics as suggested by Fairhurst and Hudson (1999), the rock samples are core-drilled and cut into two sizes: $\Phi 50\text{ mm} \times 30\text{ mm}$ and $\Phi 50\text{ mm} \times 100\text{ mm}$, and the coal samples are made into sizes of $\Phi 50\text{ mm} \times 40\text{ mm}$ and $\Phi 50\text{ mm} \times 100\text{ mm}$. The precision of these samples should meet the following requirements: (1) “the ends of the specimen shall be flat to $\pm 0.01\text{ mm}$ and shall not depart from the perpendicular to the longitudinal axis of the specimen by more than 0.001 rad (about 3.5 mm) or 0.05 in 50 mm ;” (2) “the sides of the specimen shall be smooth and straight to within 0.3 mm over the full length of the specimen” (Fairhurst and Hudson 1999). Standard samples of $\Phi 50\text{ mm} \times 100\text{ mm}$ are used to test the mechanical properties of coal and rock, respectively; composite samples shown in Fig. 2 are made by overlapped rock samples of $\Phi 50\text{ mm} \times 30\text{ mm}$ and coal samples of $\Phi 50\text{ mm} \times 40\text{ mm}$ in natural contact. Composite samples are divided into five groups, each containing three samples, as shown in Fig. 3. The compositions and sizes of the composite samples are listed in Table 1.

Testing system and process

Testing system

The testing system shown in Fig. 4 includes a loading module and strain acquisition module, and Fig. 5 shows the photographs of the instruments.



Fig. 3 Composite samples instance

Table 1 Composed part and size of composite samples

Sample group	Sample number	Sample composition	Sample size (diameter \times high)
I	1	SR-SC-SR	50.00 mm \times 99.90 mm
	2		50.20 mm \times 104.82 mm
	3		50.28 mm \times 101.00 mm
II	4	XR-SC-XR	50.22 mm \times 100.80 mm
	5		50.06 mm \times 96.50 mm
	6		50.30 mm \times 94.62 mm
III	7	LR-SC-LR	49.86 mm \times 101.80 mm
	8		50.06 mm \times 99.88 mm
	9		50.20 mm \times 102.66 mm
IV	10	JR-SC-JR	50.04 mm \times 101.58 mm
	11		50.42 mm \times 93.64 mm
	12		50.06 mm \times 97.60 mm
V	13	DR-SC-DR	50.00 mm \times 102.80 mm
	14		50.40 mm \times 105.42 mm
	15		50.40 mm \times 108.18 mm

The loading system is YAW4306 microcomputer-controlled electrohydraulic servo pressure machine, with maximum load of 3,000 kN. The resolution of the testing force indication (FS) is $1/300,000$ with $\pm 1\%$ relative error. This system can control either the applied force or the displacement of testing sample, and perform uniaxial compression, stretching, cyclic loading, and creep experiments.

Strain gages are used to detect the deformation of testing samples, and DSG9803 dynamic strain amplifier and USB8516 data acquisition instrument are adopted for strain data acquisition. DSG9803 dynamic strain amplifier provides seven magnifications through electric bridge: 10, 20, 50, 100, 200, 500, and 1,000, and can supply seven voltages: 1, 2, 3, 4, 5, 6, and 8 V. In this experiment, magnification of 200 and voltage of 4 V are chosen, and the sampling frequency of USB8516 data acquisition instrument is set to be 100 Hz.

Testing process

After testing samples are prepared, strain gages are pasted on a sample and connected with the strain data acquisition system, and then equipment debugging is made. Testing samples are then loaded under the yaw type servo compression at the loading rate of 300 N/s, until overall fracture failure occurs. The stress–strain and deformation characteristics of coal, rock and composite samples are tested, respectively.

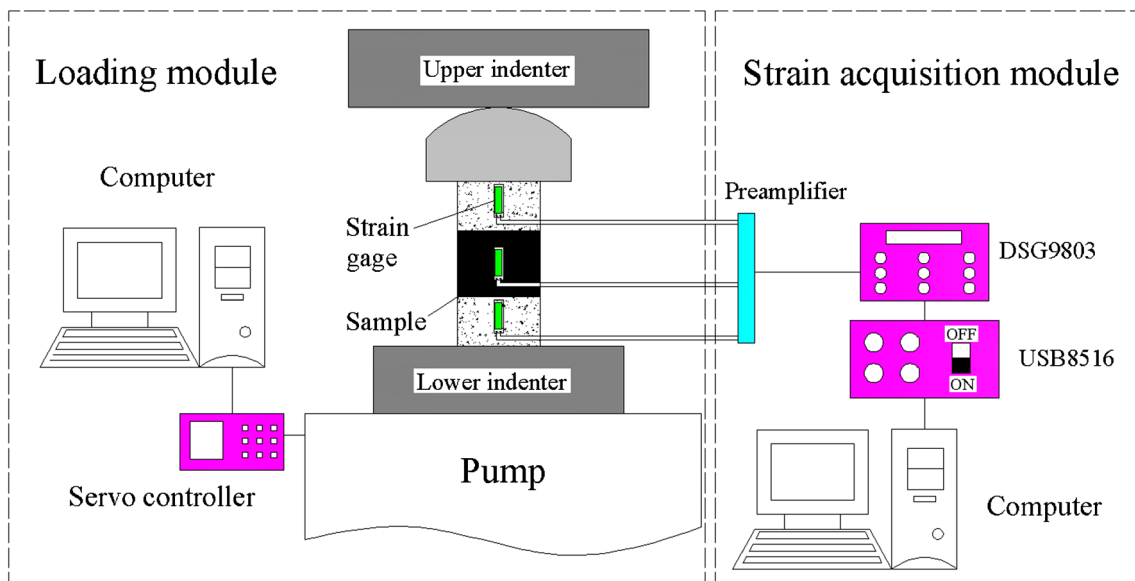


Fig. 4 Sketch map of testing system

Testing results

Stress–strain curve

The stress–strain curves of coal, rock, and composite samples are shown in Fig. 6. The curves of composite samples are located between the curves of rock and coal samples, and closer to the coal curve. A yield phase obviously exists in the curves of both composite samples and coal sample, but not in the curve of rock sample. When the coal sample is loaded above the peak stress, large deformation occurs in the sample before its load-bearing capacity is completely lost; in contrast, the composite samples had little deformation after the peak stress is reached and before fracture failure occurs, suggesting that the composite samples have a higher rate of fracture than the coal sample.

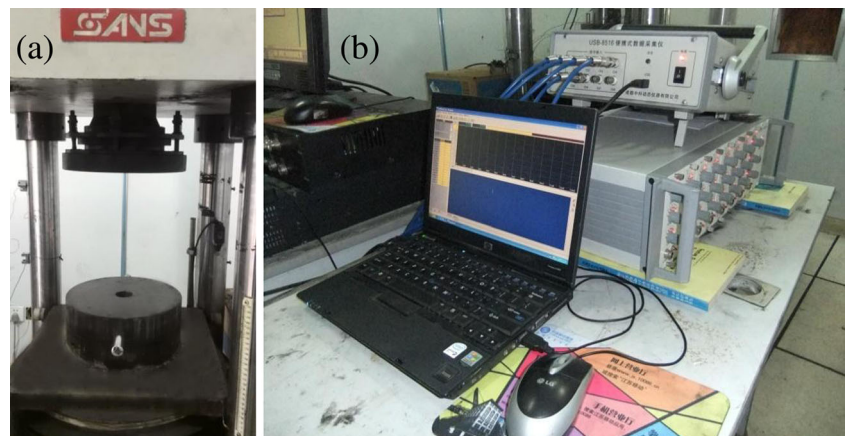
For the composite samples with different rock strengths, with the increase of rock strength, the

variation of strain gets smaller from the yield point to peak pressure, and the time for the growth of internal cracks to breakdown gets shorter. Figure 6 also shows that the process from the yield point to the peak stress point is accompanied by obvious nonlinear behavior and takes a longer time for the composite samples with lower rock strengths, such as group I (rock strength of 38.66 MPa) and group II (rock strength of 57.86 MPa). With increasing rock strength, this process takes a shorter time.

Failure mode

Final failure modes of composite samples with different rock strengths are shown in Fig. 7. The fracture surfaces of some composite samples are not retained completely, since the residual strength of coal can no longer support the weight of the roof rock. Figure 7 also shows that

Fig. 5 Physical experiment system diagram. **a** Yaw type servo press. **b** Strain acquisition system



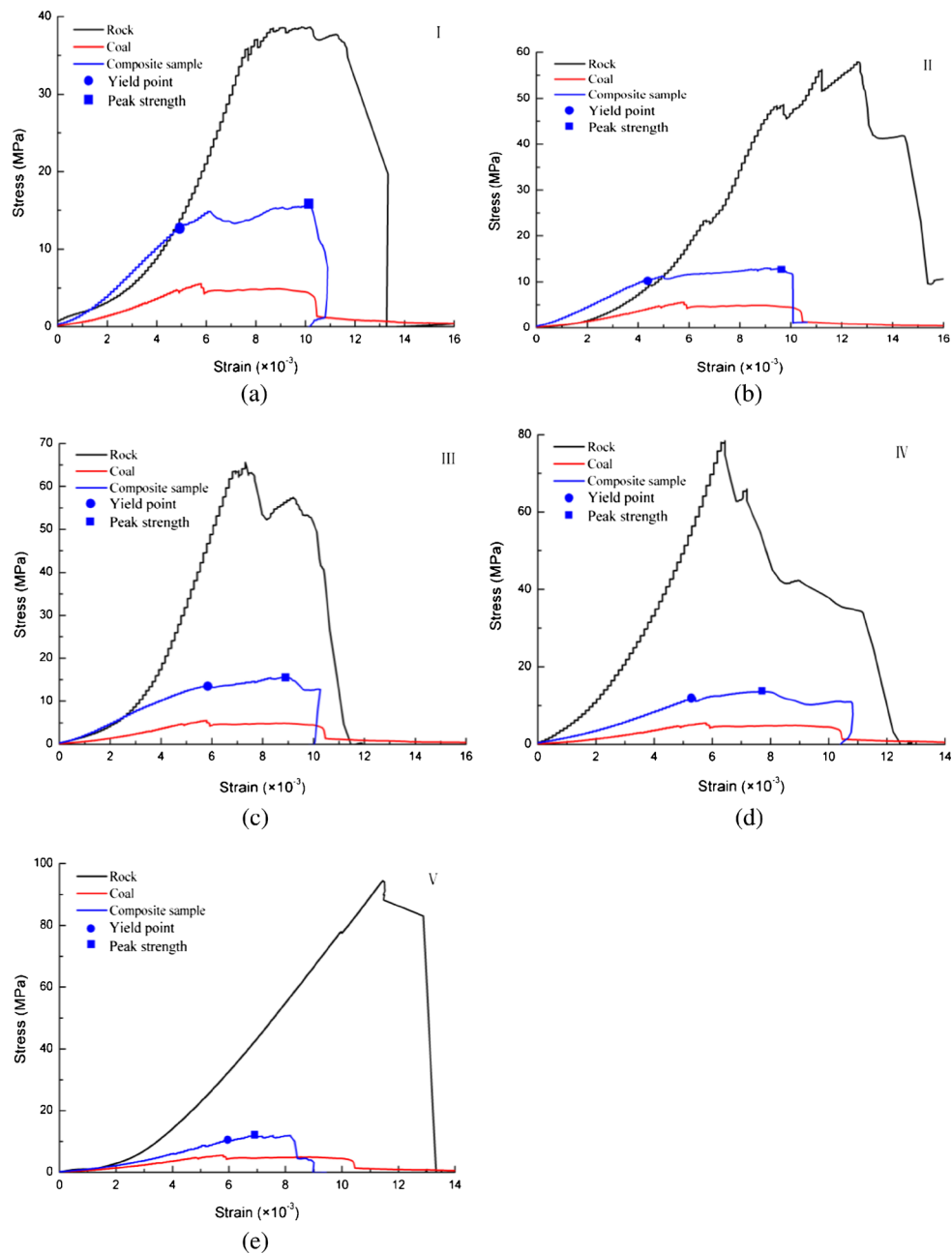


Fig. 6 Stress–strain curves

the coal bodies are broken more thoroughly and seriously than the rock bodies. The lower part of the coal body is tapered, indicating that the coal body was subject to shear stress and failed by shear fracture, and suggesting that the “X”-type shearing fracture surface must have been formed inside the coal before failure. The angle between the shear fracture surface and the end face, β , turns larger with the increase of rock strength. Three vertical cracks are also observed in the coal body of group I, and one vertical crack in group III, indicating the occurrence of splitting fracture. It can

be inferred from the shear fracture surface and tensile cracks that shear fracture mainly occurs before splitting, and the final destruction of the coal is dominantly splitting, as shown in Fig. 7f.

Failure modes of the rock part are shown in Fig. 8. When the composite samples, groups I and II, fail, the cracks in the coal part extend to the rock part, as shown in panels a and b of Fig. 8. The rock is broken into two parts, and the fracture surface is smooth, suggesting the occurrence of tensile fracture. In groups III and IV, only one composite sample has ruptured rock part each, as

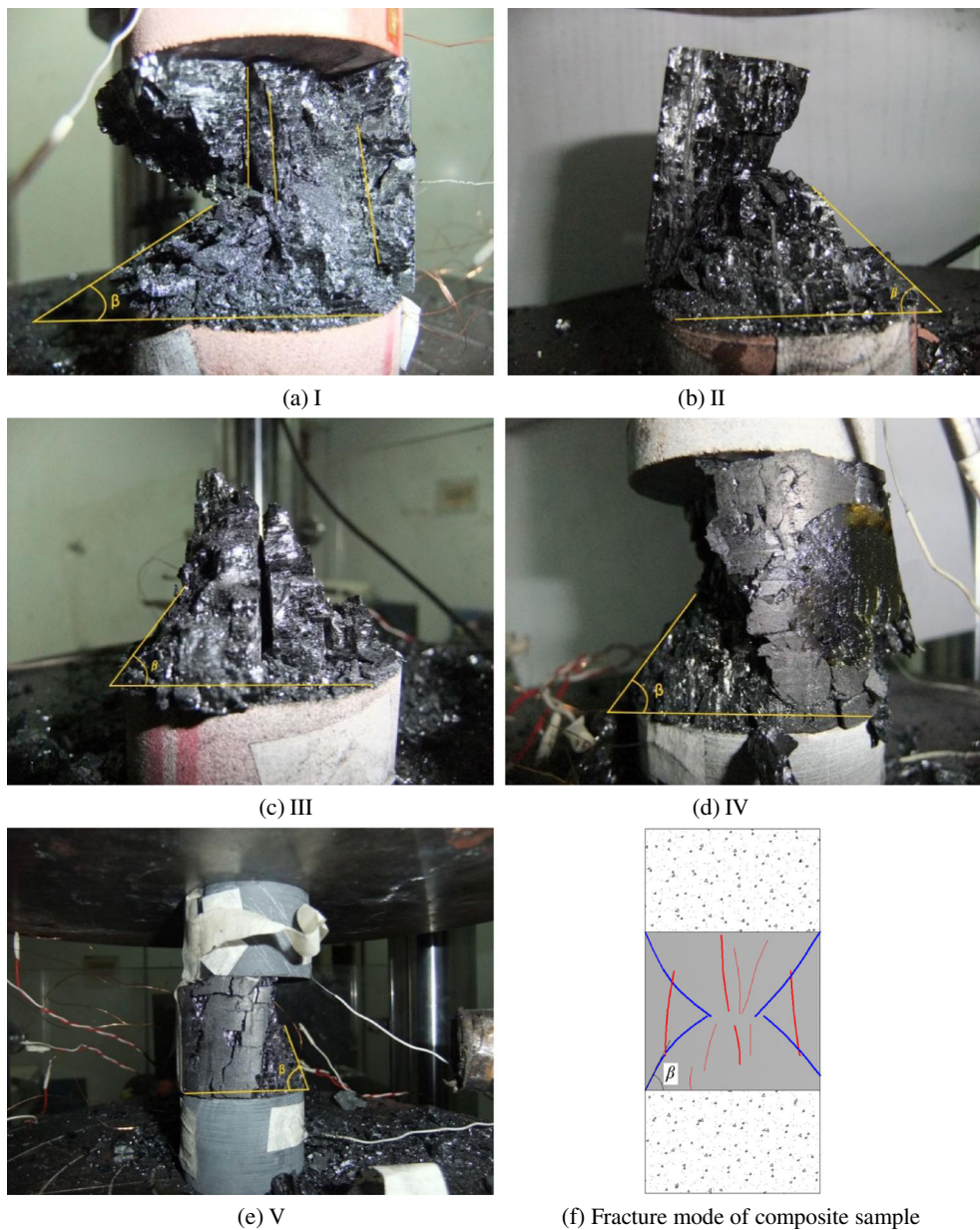


Fig. 7 Failure mode of composite samples **a I**, **b II**, **c III**, **d IV**, **e V**, and **f** Fracture mode of composite sample

shown in panels c and d of Fig. 8. It suggests that composite samples with higher rock strength could be

broken when a large amount of energy is released during coal–mass fracture. The rock parts of the

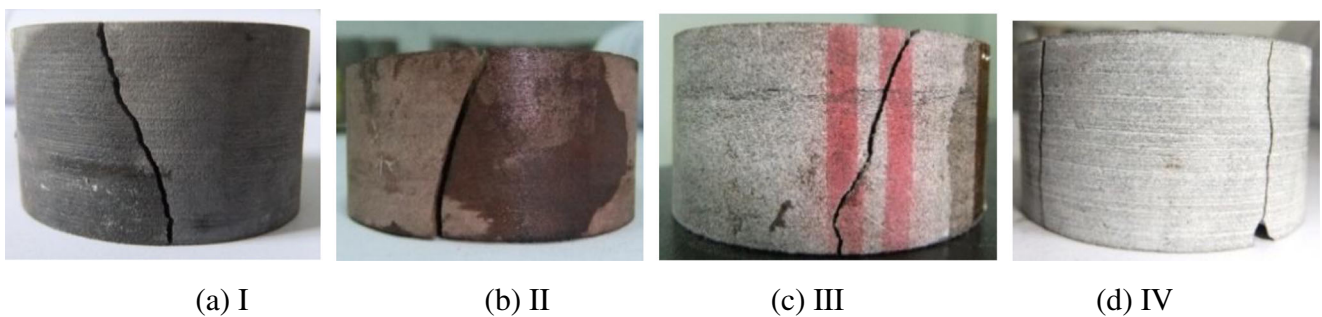


Fig. 8 Failure mode of roof rock **a I**, **b II**, **c III**, and **d IV**

samples in group V are complete, so they are not included in Fig. 8.

Variation of strain in composite samples

Variation of strain in the rock and coal parts during the loading process is shown in Fig. 9. The strain of the coal and rock parts increases gradually with the increasing of load, and the strain of the coal part is larger than that of the rock part. By the time of fracture failure, the strain of both parts changes greatly, and the coal part also has larger change than the rock part, suggesting that cracking deformation mainly occurs in the coal part

during the loading process. For group I with rock strength of 38.66 MPa, the strain of the coal part is about two times of the strain of the rock part before fracture failure, and the strain rate of both parts are almost equal. Groups II and III have greater rock strength, 57.86 and 65.54 MPa respectively, so the difference between the strain of the coal and rock parts is even larger, and the strain rate of the coal part is larger than that of the rock part. For groups IV and V with even greater rock strength, 83.21 and 94.57 MPa respectively, both the strain and strain rate of the coal part are far larger than those of the rock part, and the strain of the rock part is very small, as shown in panels d and e of Fig. 9.

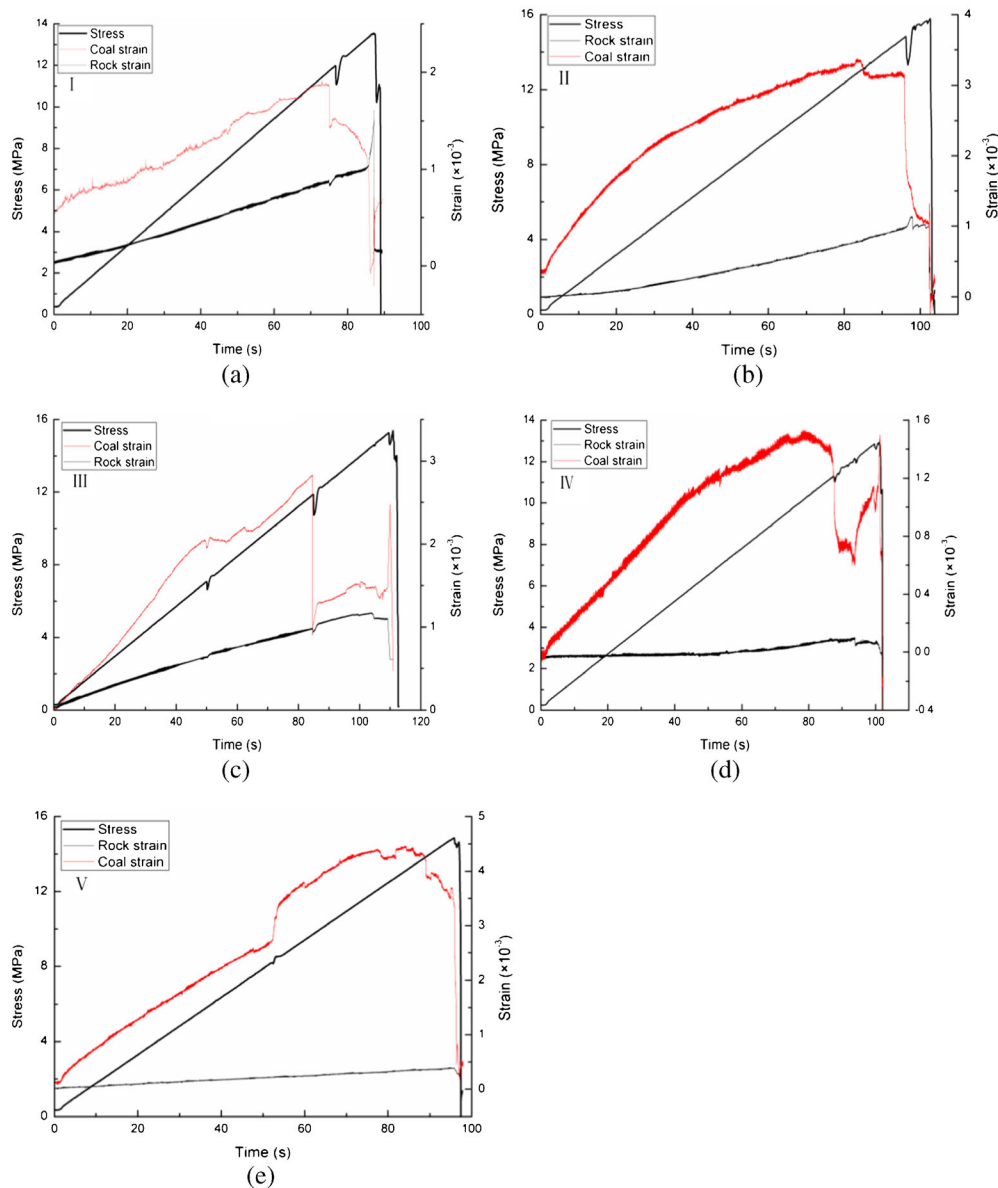


Fig. 9 Strain change laws of composite samples

Analysis and discussion

Strength of composite samples under uniaxial compression

The force acting on the deformed rock–coal–rock composite samples under uniaxial compression can be schematically analyzed in Fig. 10 (Tang 1993; Chen et al. 1997); in the figure, u_r , u_c , u_f , and u represents deformation of the roof, the coal, the floor, and the composite sample, respectively; P denotes the applied external load. Before the occurrence of fracture failure, the loading process can be regarded as a series of static or quasi-static states, and force balance in the vertical direction satisfies:

$$\sigma_r = \sigma_c = \sigma_f = \sigma = P/A \tag{1}$$

where σ_r , σ_c , σ_f , σ denotes the vertical stress of the roof rock, coal, floor rock, and composite sample, respectively; A denotes the cross-sectional area of the composite sample. In the process of quasi-static loading, the load on the coal part and the rock part are the same. When the external load reaches the uniaxial compressive strength of the coal part, fracture failure of the coal part occurs, and the whole composite sample loses load-bearing capacity; therefore, the uniaxial compressive strength of the composite sample is determined by the strength of the coal part. Comparison of peak strength of the five groups of composite samples is shown in Fig. 11. Among the five groups, the difference in the maximum strength is 0.64 MPa, and the difference in the minimum strength is 1.78 MPa. The difference between the maximum and minimum value of average strength is 1.67 MPa. Considering individual deviations in the samples, the strength of the composite samples can be generally regarded as the same when the rate of loading is equal.

Comparison of the uniaxial compressive strength of the composite samples and coal sample shows that the strength

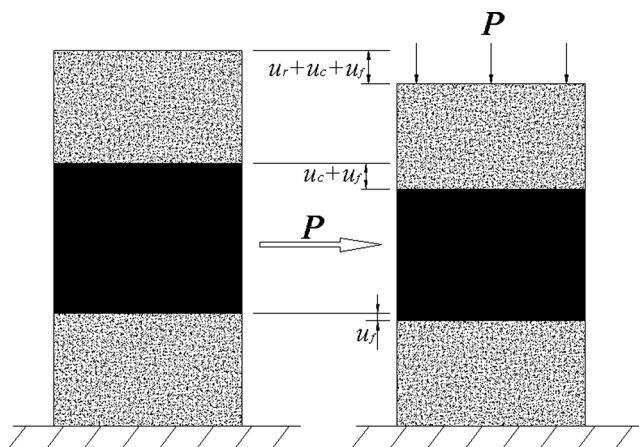


Fig. 10 Sketch map of composite sample force analysis

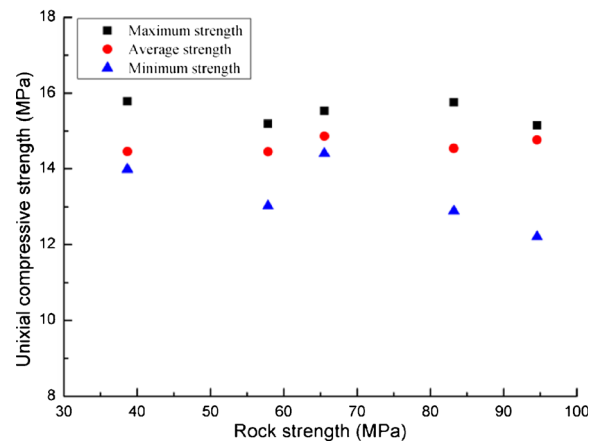


Fig. 11 Strength comparison

of composite sample is much higher than that of coal sample, which agrees with former research results (Li et al. 2005; Huang and Liu 2013). Tuncay and Hasancebi (2009) found that the height-diameter ratio is highly correlated to uniaxial compressive strength; when the height-diameter ratio is less than 2, the strength of the testing sample increases significantly. The height-diameter ratio of the coal parts in the composite samples in this study is just 0.8, so their uniaxial compressive strength must be higher than the standard coal sample whose height-diameter ratio is 2. Therefore, the uniaxial compressive strengths of coal samples with a size of $\Phi 50 \text{ mm} \times 40 \text{ mm}$ (height-diameter ratio of 0.8) are tested for comparison, and the result is shown in Fig. 12. Compared to the standard coal sample, the uniaxial compressive strength of the $\Phi 50 \text{ mm} \times 40 \text{ mm}$ coal sample has improved and is almost equal to the strength of composite sample. Moreover, the end effect caused by the rock–coal interface has little influence on uniaxial strength (Wawersik and Fairhurst 1970; Tang, et al. 2000). It is concluded that the higher uniaxial compressive strength of composite sample results from the reduced height-diameter ratio of its coal part.

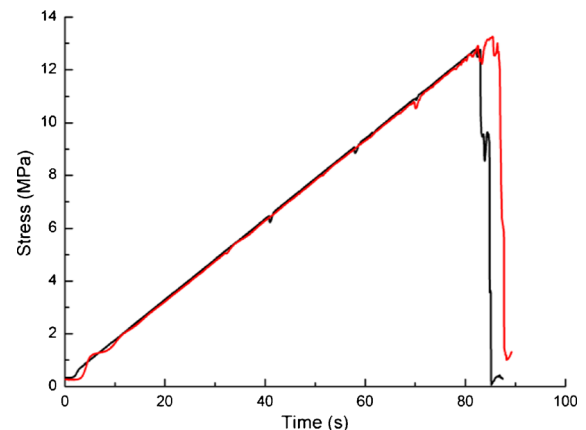


Fig. 12 Stress curve of single coal sample of $\varphi 50 \text{ mm} \times 40 \text{ mm}$

Rock strength and failure mode of composite samples

In order to discover the relationship between rock strength and failure modes, the stress and strain of the rock and coal part of the composite sample is analyzed. An element is taken at the interface of coal and rock, as shown in Fig. 13. Its upper part belongs to the rock unit, and its lower part belongs to the coal unit. The horizontal strain of both parts can be derived (Tan et al. 1994):

$$\varepsilon_{2r} = \varepsilon_{3r} = \mu_r \frac{\sigma_r}{E_r} \tag{2}$$

$$\varepsilon_{2c} = \varepsilon_{3c} = \mu_c \frac{\sigma_c}{E_c} \tag{3}$$

where ε_{2r} , ε_{3r} , ε_{2c} , and ε_{3c} are the strain of the rock and coal part in the horizontal direction, respectively; μ_r and μ_c is the Poisson’s ratio of rock and coal, respectively; σ_r and σ_c are the axial stress in the rock and the coal part, respectively, and E_r and E_c are the elastic modulus of rock and coal, respectively. The Poisson’s ratio and elastic modulus of rock and coal satisfy:

$$\mu_r < \mu_c, E_c < E_r$$

Under uniaxial compression, $\sigma_r = \sigma_c$, so we have

$$\varepsilon_{2r} < \varepsilon_{2c}$$

suggesting that the strain in the horizontal direction in the rock part differs from that in the coal part. It can be further inferred that frictional force must exist on the rock–coal

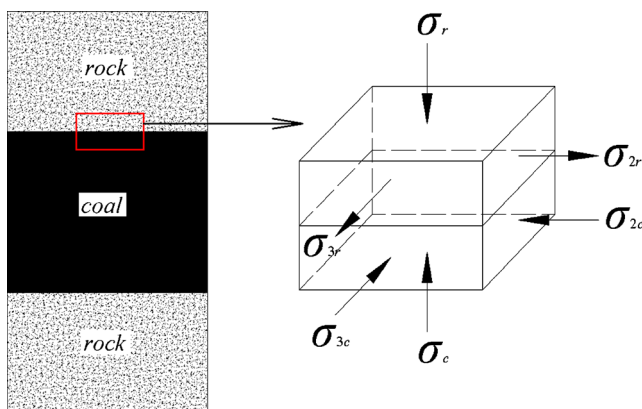


Fig. 13 Element at the interface between coal and rock

interface to restrict the deformation of rock and coal, and this frictional force can be expressed as

$$\sigma_{2r} = f_{rc} \cdot \sigma_r \tag{4}$$

where f_{rc} is the coefficient of friction between coal and rock surfaces, the friction coefficient in the interface between coal and rock varies with the distance from the interface center. The relative displacement is different in the interface of coal and rock. The relative displacement is zero in the center of the interface, and it increases far away from center. Therefore, the coefficient and friction vary with the distance from the center of the specimen.

The theoretical strength of the element can be predicted according to the Mohr–coulomb criterion (Tan et al. 1994):

$$\sigma_1 = \frac{1 + \sin\varphi}{1 - \sin\varphi} \sigma_3 + R_c \tag{5}$$

where σ_1 and σ_3 are the vertical and horizontal ultimate principal stress, respectively; φ is the internal frictional angle of the interface; and R_c is the uniaxial compressive strength. When no friction exists on the interface of rock and coal, we have

$$\sigma_1 = R_c$$

Figure 13 also shows that

$$\sigma_1 = \sigma_r, \sigma_3 = -\sigma_{2r}$$

The strength of the rock part in the vicinity of the coal–rock interface is

$$\sigma_{rc} = \frac{R_{rc}}{1 + \frac{1 + \sin\varphi_r f_{rc}}{1 - \sin\varphi_r}} \tag{6}$$

Similarly, the uniaxial compressive strength of the coal part is

$$\sigma_{cc} = \frac{R_{cc}}{1 - \frac{1 + \sin\varphi_c f_{rc}}{1 - \sin\varphi_c}} \tag{7}$$

Formulas (5) and (6) show that near the coal–rock interface on the rock side, the uniaxial compressive strength is smaller than that away from the interface area; however, on the coal

side, the uniaxial compressive strength is greater than that away from the interface area.

Under uniaxial compression, the stress state in the composite sample can be shown in Fig. 14. Near to the coal–rock interface, the magnitude of the horizontal compressive stress in the coal body equals the horizontal tensile stress in the rock body, and the direction is opposite; at the interface, both stresses reach the maximum, σ_{2r} , and decrease toward the center of the coal or rock gradually, and eventually disappear.

In the region under the influence of end effect, the coal elements are in triaxial compression, so the coal is not easy to fracture; the coal in the middle part is still subject to uniaxial stress, and the radial tensile stress generated under compression, so tensile rupture is easy to occur, and the type “X” or “hourglass” crack may be formed in the coal body after fracture failure.

Generally, the rock with higher uniaxial compressive strength has greater elastic modulus and lower Poisson’s ratio, so the relative deformation between rock and coal gets larger. Accordingly, the friction between the coal–rock interfaces is greater and the region under the influence of end effect in the coal body gets larger, so the angle β between the shear fracture surface and horizontal end face is bigger.

After the load is increased to the peak strength of coal, the internal cracks outside the zone subject to the end effect grow and link up into fracture parallel to the axial stress. At the same time, a large amount of energy is consumed and released. At this moment, the cracks

will expand to both ends and across to the rock, and if the strength of rock is not high enough, fracture failure of the rock may occur. This phenomenon has been observed in the experiment shown in Fig. 8.

Rock strength and characteristics of deformation

As shown in Fig. 10, the deformation of composite sample is

$$u_r + u_c + u_f = u \quad (8)$$

The stiffness of the composite sample is

$$\begin{aligned} \lambda &= \frac{P}{u} = \frac{P}{u_r + u_c + u_f} = \frac{P}{\frac{P}{\lambda_r} + \frac{P}{\lambda_c} + \frac{P}{\lambda_f}} \\ &= \frac{\lambda_r \lambda_c \lambda_f}{\lambda_r \lambda_c + \lambda_r \lambda_f + \lambda_c \lambda_f} \end{aligned} \quad (9)$$

where λ , λ_r , λ_c , and λ_f are the stiffness of the composite sample, roof rock, coal bed, and floor rock, respectively. According to the relationship between elastic modulus and stiffness, the following equation can be obtained:

$$E = \lambda h / A \quad (10)$$

where E is the specimen modulus; h is the specimen height; and A is the cross-sectional area of the specimen. Supposing that the lithology and size of the roof and floor rock are the same, the elastic modulus of composite sample can be obtained as follows:

$$E = \frac{E_r E_c A}{E_r h_c + 2E_c h_r} \cdot \frac{h}{A} = \frac{E_c h}{h_c + 2h_r E_c / E_r} \quad (11)$$

where E_r and E_c are the elastic modulus of rock and coal and h_r and h_c are the height of the rock and coal bed. According to this formula, the elastic modulus of the composite sample is related to the elastic modulus and height of the rock and coal.

The elastic moduli of coal and rock are obtained from the mechanical test result shown in Table 2. The elastic modulus of composite samples can be independently obtained from either the result of their mechanical test or Eq. (11), as shown in Fig. 15. According to Fig. 15, the elastic modulus of composite samples derived from Eq. (11) is larger than that obtained from the test result, but with identical trend of variation.

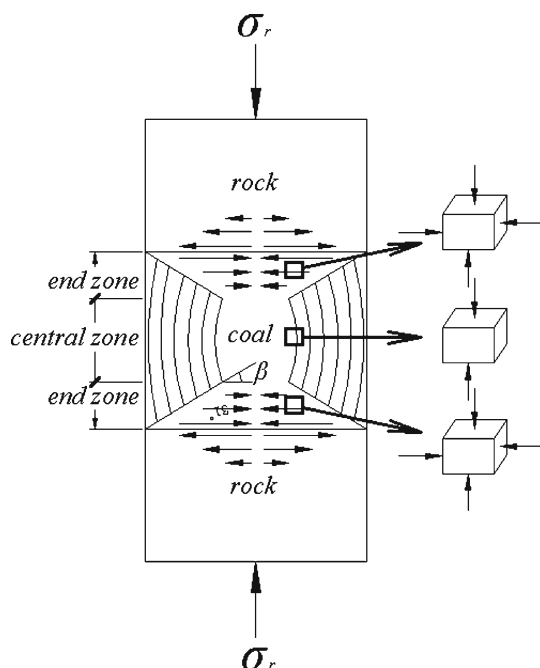


Fig. 14 Stress state and failure modes inside composite sample

Table 2 Elastic modulus of rock and coal

Test No.	E (GPa)	Average value (GPa)	Test No.	E (GPa)	Average value (GPa)
I-R-1	8.53	6.37	IV-R-1	21.74	17.85
I-R-2	5.79		IV-R-2	18.02	
I-R-3	4.79		IV-R-3	13.79	
II-R-1	10.41	10.80	V-R-1	16.56	18.51
II-R-2	11.20		V-R-2	23.16	
II-R-3	10.78		V-R-3	15.81	
III-R-1	11.54	11.84	Coal-1	1.57	1.77
III-R-2	11.06		Coal-2	1.16	
III-R-3	12.93		Coal-3	2.57	

The ratio of the strain of coal and rock can be also calculated. According to Eq. (1),

$$E_r \varepsilon_r = E_c \varepsilon_c \tag{12}$$

and

$$\frac{\varepsilon_c}{\varepsilon_r} = \frac{E_r}{E_c} \tag{13}$$

where ε_r and ε_c represent the strain of coal and rock, respectively. The calculated ratio of strain in the elastic phase and the experimental results are both shown in Fig. 16. The calculated strain ratio and the experimental results rise linearly with rock strength and have identical trend.

According to Figs. 15 and 16, the elastic modulus of composite samples derived from Eq. (11) and the strain ratio derived from Eq. (13) are larger than that obtained

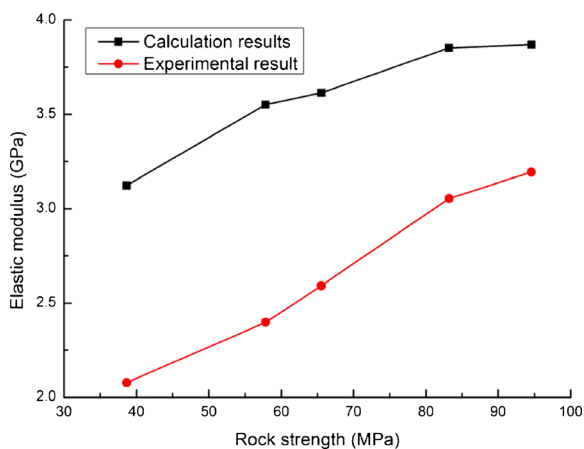


Fig. 15 Elastic modulus

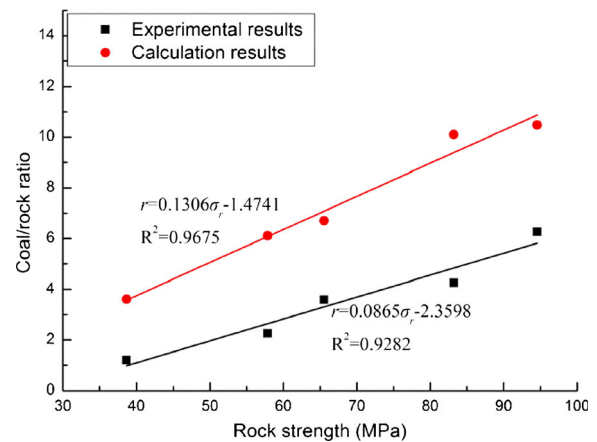


Fig. 16 Strain ratio of calculation and experiment

from the test result because the mechanical properties of coal and rock are different.

The stress–strain curves of rock and coal can be divided into compaction phase and elastic phase before they yield. The compaction phase and elastic phase of coal and rock are not synchronous because of the different mechanical properties of coal and rock, which lead to the differences between experimental results and calculated results. From the stress–strain curves shown in Fig. 6, it is obtained that the deformation phases of the coal are similar with the composite samples. They have little influence on the differences between experimental results and calculated results, so the influence of deformation phase discrepancies between rock and composite sample on the differences between experimental results and calculated results is mainly analyzed in this paper.

Take group I as an example; the stress–strain curves of rock and composite sample of group I before composite sample yielded are shown in Fig. 17. OA₁ and OB₁ are the

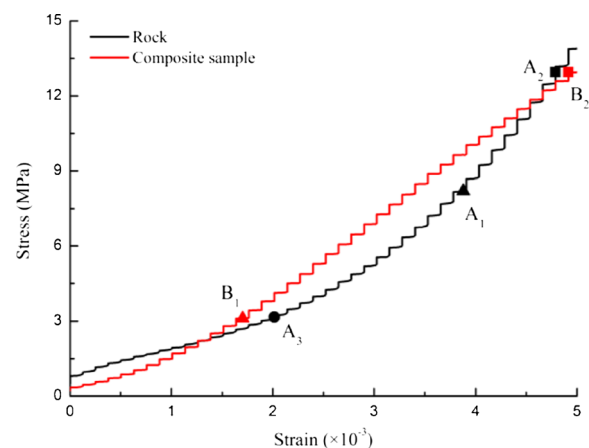


Fig. 17 Stress–strain curves of rock and composite sample before composite sample yield

compaction phase of stress–strain of rock and composite sample, respectively; A_1A_2 and B_1B_2 are the elastic phase of stress–strain of rock and composite sample, respectively. A_3A_2 in the stress–strain of rock is corresponding to B_1B_2 in the stress–strain of composite sample, so the secant modulus of A_3A_2 determines the elastic modulus of composite sample. From the stress–strain curves, the secant modulus of A_3A_2 is obviously less than the elastic modulus of rock. Therefore, the experimental results are less than the calculated results from Eqs. (11) and (13). The other samples, groups II, III, IV, and V, are similar with group I.

Although choosing the elastic moduli of rock and coal to analyze the elastic modulus and deformation rules of composite sample could lead to little difference with the experimental results, the secant modulus of A_3A_2 is close to the elastic modulus of rock. Therefore, the model established in the paper can be used to qualitatively compare and analyze the elastic modulus and deformation rule of composite sample.

Conclusions

In this paper, the effects of rock strength on the mechanical behavior of rock–coal–rock composite samples are studied through laboratory experiments and theoretical analysis. The following statements can be concluded:

- (1) The composite samples have stress–strain curve between that of rock and coal, and closer to coal. A nonlinear phase obviously exists in the stress–strain curves of composite samples and coal sample. Increase of rock strength can significantly shorten the time for the composite samples to go from the yield point to peak strain point. The strength properties of composite samples depend mostly on the coal part, and the effect of rock strength is negligible.
- (2) The composite samples demonstrate conjugate X-shaped shear fracture and splitting fracture in the coal. The angle between the shear fracture surface and end face increases with rock strength, which can be explained by the influence of end effect caused by the difference between the elastic modulus of coal and rock. When rock strength is low, splitting fracture in the coal body expands to the rock.
- (3) With the increase of rock strength, the peak strain of composite samples decrease, and the difference between either the strain or strain rate of rock and coal becomes greater. This characteristic of deformation is considered to be related to the variation of the elastic modulus of composite sample, which is dependent on the elastic modulus and height of the rock and coal bed.

Acknowledgments This research is financially supported by National Science and Technology Support Program (2012BAK09B01-04), the Youth Science Foundation of the National Natural Science Foundation of China (51304205) and High Lever Paper Special Fund Supported by China University of Mining and Technology (2012LWBZ08).

References

- Bai QH, Tu SH, Zhang XG et al (2013) Numerical modeling on brittle failure of coal wall in longwall face—A case study. *Arab J Geosci*. doi:10.1007/s12517-013-1181-1
- Bieniawski ZT, Denkhaus HG, Vogler UW (1969) Failure of fractured rock. *Int J Rock Mech Min Sci Abstr* 3:331–341
- Chen ZH, Tang CA, Huang RQ (1997) A double rock sample model for rockbursts. *Int J Rock Mech Min Sci* 6:991–1000
- Cook NGW (1965) The failure of rock. *Int J Rock Mech Min Sci Abstr* 4:389–403
- Deng XB, Hu HJ, Xu G et al (2012) Numerical simulation for burst failure of two-body rock structure. *J Min Saf Eng* 6:833–839 (in Chinese)
- Dou LM, Lu CP, Mu ZL et al (2006) Experimental study of rock burst tendency of coal–rock compound samples. *Progress Saf Sci Technol* 6:1729–1732
- Fairhurst CE, Hudson JA (1999) International society for rock mechanics commission on testing methods: draft ISRM suggested method for the complete stress–strain curve for intact rock in uniaxial compression. *Int J Rock Mech Min Sci* 36:279–289
- Guo DM, Zuo JP, Zhang Y et al (2011) Research on strength and failure mechanism of deep coal–rock combination bodies of different inclined angles. *Rock Soil Mech* 5:1333–1339 (in Chinese)
- He MC, Xie HP, Peng SP et al (2005) Study of rock mechanics in deep mining engineering. *Chin J Rock Mech Eng* 16:2803–2813 (in Chinese)
- Hosseini N, Oraee K, Shahriar K et al (2013) Studying the stress redistribution around the longwall mining panel using passive seismic velocity tomography and geostatistical estimation. *Arab J Geosci* 6(5):1407–1416
- Huang BX, Liu JW (2013) The effect of loading rate on the behavior of samples composed of coal and rock. *Int J Rock Mech Min Sci* 61:23–30
- Lama RD, Bodziony J (1998) Management of outburst in underground coal mines. *Int J Coal Geol* 35:83–115
- Li JQ, Qi QX, Mao DB et al (2005) Discussion on evolution method of bursting liability with composite model of coal and rock. *Chin J Rock Mech Eng, Supp.1*: 4805–4810 (in Chinese)
- Lin P, Tang CA, Chen ZH et al (1999) Numerical and experimental study of deformation and failure behavior in a double rock specimen system. *Earthquake* 4:413–418 (in Chinese)
- Liu B, Yang RS, Guo DM et al (2004) Burst-prone experiments of coal–rock combination at -1100 m level in Suncun coal mine. *Chin J Rock Mech Eng* 14:2402–2408 (in Chinese)
- Liu CL, Tan ZX, Deng KZ et al (2013) Synergistic instability of coal pillar and roof system and filling method based on plate model. *Int J Rock Mech Min Sci* 23:145–149
- Lu CP, Dou LM, LI HM (2009) Research on the evaluation of relieve-shot effect by microseism. *Controlling Seism Hazard Sustain Dev Deep Mines* 1:307–312
- Lu CP, Dou LM, Wang YF et al (2010) Microseismic effect of coal materials rockburst failure induced by hard roof. *Chin J Geophys-Chin Ed* 2:450–456
- Paul A, Singh AP, John P et al (2012) Validation of RMR-based support design using roof bolts by numerical modeling for underground coal mine of Monnet Ispat, Raigarh, India—a case study. *Arab J Geosci* 5(6):1435–1448

- Qin SQ, Jiao JJ, Tang CA et al (2006) Instability leading to coal bumps and nonlinear evolutionary mechanisms for a coal-pillar-and-roof system. *Int J Solids Struct* 43:7407–7423
- Seidel JP, Haberfield CM (2005) A theoretical model for rock joints subjected to constant normal stiffness direct shear. *Int J Rock Mech Min Sci* 39:539–553
- Shabanimashcool M, Li CC (2012) Numerical modelling of longwall mining and stability analysis of the gates in a coal mine. *Int J Rock Mech Min Sci* 51:24–34
- Singh AK, Singh R, Maiti J et al (2011) Assessment of mining induced stress development over coal pillars during depillaring. *Int J Rock Mech Min Sci* 48:805–818
- Tan XS, Xian XF, Zheng DF et al (1994) Theory and its application of composite rock mechanics. China Coal Industry Publishing House, Beijing (in Chinese)
- Tang CA (1993) Catastrophe in rock unstable failure. China Coal Industry Publishing House, Beijing
- Tang CA, Tham LG, Lee PKK et al (2000) Numerical studies of the influence of microstructure on rock failure in uniaxial compression—part II: constraint, slenderness and size effect. *Int J Rock Mech Min Sci* 37:571–583
- Tuncay E, Hasancebi N (2009) The effect of length to diameter ratio of test specimens on the uniaxial compressive strength of rock. *Bull Eng Geol Environ* 68:491–497
- Vesela V (1996) The investigation of rockburst focal mechanisms at lazy coal mine, Czech Republic[J]. *Int J Rock Mech Min Sci Geomech Abstr* 33(8):380A
- Wawersik WR, Fairhurst C (1970) A study of brittle rock fracture in laboratory compression experiments. *Int J Rock Mech Min Sci & Abstr* 5:561–564
- Xie HP, Chen ZH, Zhou HW et al (2005) Study on two-body mechanical model based on interaction between structural body and Geo-body. *Chin J Rock Mech Eng* 9:1457–1464 (in Chinese)
- Zhang ZT, Liu JF, Wang L et al (2012) Effects of combination mode on mechanical properties and failure characteristics of the coal–rock combinations. *J China Coal Soc* 10:1677–1681 (in Chinese)
- Zhang N, Zhang NC, Han CL et al (2014) Borehole stress monitoring analysis on advanced abutment pressure induced by long wall mining. *Arab J Geosci* 7(2):457–463
- Zuo JP, Xie HP, Wu AM et al (2011a) Investigation on failure mechanisms and mechanical behaviors of deep coal–rock single body and combined body. *Chin J Rock Mech Eng* 1:84–92 (in Chinese)
- Zuo JP, Xie HP, Meng BB et al (2011b) Experimental research on loading-unloading behavior of coal–rock combination bodies at different stress levels. *Rock Soil Mech* 5:1287–1296 (in Chinese)